Eur. Phys. J. B **61**, 397–403 (2008)
DOI: 10.1140/epjb/e2008-00107-0

THE EUROPEAN PHYSICAL JOURNAL B

First-principles study of high pressure phase transformations in Li_3N

Y. Yan[1,2], J.Y. Zhang[1], T. Cui[1], Y. Li[1], Y.M. Ma[1,a], J. Gong[2], Z.G. Zong[2], and G.T. Zou[1]

[1] National Lab of Superhard Materials, Jilin University, Changchun 130012, P.R. China
[2] Applied Physics Institute, Changchun University, Changchun 130022, P.R. China

Received 26 September 2007 / Received in final form 27 January 2008
Published online 13 March 2008 –

Abstract. The lattice dynamics of lithium nitride (Li_3N) under high pressure are extensively investigated to probe its phase transformations by using the pseudopotential plane-wave method within the density functional theory. A new second order $\alpha \rightarrow \alpha'-Li_3N$ phase transition is identified for the first time. The newly proposed $\alpha'-$phase possesses a hexagonal symmetry with four ions in the unit cell having a space group of $P-3m1$. Further enthalpy and phonon calculations support the existence of this phase, which stabilizes in a narrow pressure range of 2.8 – 3.6 GPa at zero temperature. Upon further compression, transitions to denser packed phases of $\beta-$and $\gamma-Li_3N$ are typical first order. The analysis of the electronic densities of states suggests that all the high pressure modifications of Li_3N are insulators and, interestingly, the typical behavior of compression is to broaden the band gap.

PACS. 62.50.-p High-pressure effects in solids and liquids

1 Introduction

Lithium nitride, Li_3N, is the only known thermodynamically stable alkali metal nitride and is one of the most ionic of all known nitrides. There have been considerable interests in the static and dynamic properties of Li_3N [1–3]. This material is a superionic conductor via vacancy-induced Li^+ diffusion within the Li_2N layers [4–6]. Its potential for use as an electrolyte in Li-based batteries [7], a hydrogen storage medium [8–11], and a component in the synthesis of GaN [12] have prompted several studies including an investigation into its behavior at high pressure [13]. It is known that Li_3N crystallizes in a hexagonal structure [7,14], $\alpha-Li_3N$, with four ions per unit cell at ambient conditions. The unit-cell dimensions are $a = 3.648$ Å and $c = 3.875$ Å [15] with the symmetry point group of D_{6h} (space group P6/mmm). The nitrogen exists in an anomalous multiply charged (N^{3-}) states [16,17] which is stable only because of its crystal environment—a hexagonal bipyramid of Li^+ ions. This structure consists of Li_2N layers, widely separated and connected by one lithium atom per unit cell occupying a site between the nitrogen atoms in adjacent layers [7,14].

At around 0.6 GPa and room temperature, $\alpha-Li_3N$ was observed to transform into a layered hexagonal structure ($\beta-Li_3N$, $P6_3/mmc$) with BN-like honeycomb LiN layers [15]. In this structure, every nitrogen ion binds an additional lithium atom above and below the plane and, unlike the Li_2N layers in $\alpha-Li_3N$, adjacent LiN layers are shifted relative to one another. $\beta-Li_3N$ is metastable at ambient pressure and is typically found mixed with $\alpha-Li_3N$ phase. With increasing pressure a further phase transition to a cubic structure ($\gamma-Li_3N$)—$Fm\bar{3}m$ at 27.6 GPa [18] — has previously been predicted by a two-step procedure consisting of an exploration of the energy landscapes of chemical systems at various pressures using global optimization techniques, followed by a local optimization with ab initio methods. Recently, it is proved by Lazicki et al. [19] that $\beta-Li_3N$ indeed transforms to $\gamma-Li_3N$, but in the pressure range of 36–45 GPa. The $\gamma-Li_3N$ phase is uncommonly stable up to at least 200 GPa and quite compressible in this pressure regime, making it a good candidate for an internal pressure standard.

In the present work, the lattice dynamics of Li_3N within the three polymorphs ($\alpha-$, $\beta-$, and $\gamma-$phases) have been extensively studied through ab initio calculations to understand the physically driven mechanisms of the phase transitions.

2 Theoretical methods

Pseudopotential plane-wave ab initio calculations are carried out within the framework of density functional theory [20], through the Quantum-ESPRESSO package [21]. The generalized gradient approximation (GGA) exchange-correlation functional is employed [22]. The Troullier-Martins [23] norm-conserving scheme is used to generate

[a] *Correponding Author:* e-mail: mym@jlu.edu.cn

the pseudopotentials for Li and N with the valence configurations of $2s^1$, and $2s^2 2p^3$, respectively. A nonlinear core-correction to the exchange-correlation energy functional for Li is introduced to compensate the incomplete description of valence states within 2s electrons. The core radii of 2.0 a.u. and 1.2 a.u. for Li and N, respectively, are chosen to be sufficiently small to guarantee the core non-overlapping under compression in this study. Convergence tests give the choices of the kinetic energy cutoff E_{cutoff} of 110 Ry and $8\times8\times6$, $12\times12\times12$, $8\times8\times4$, and $8\times8\times8$ Monkhorst-Pack [24] (MP) k grids for $\alpha-, \alpha'-, \beta-$, and $\gamma-Li_3N$ phases in the electronic Brillouin zone (BZ) integration, respectively. As a consequence, the calculated total energy is well converged within 1.0×10^{-3} Ry/f.u. The phonon frequencies are calculated using the density functional linear-response method [25–27]. Through this approach, the dynamical matrices are calculated by determining the static linear response of the electrons for a periodic lattice perturbation. The $8\times8\times6$, $12\times12\times12$, $12\times12\times6$, and $10\times10\times10$ MP k meshes used in the phonon calculations ensure the convergence of phonon frequencies within 0.01 THz, and the $4\times4\times3$, $4\times4\times4$, $4\times4\times2$, and $4\times4\times4$ q meshes for the four polymorphs, respectively, are employed to interpolate the force constants in deriving the phonon dispersion curves.

3 Results and discussions

The theoretical equilibrium lattice constant is determined by fitting the total energy as a function of volume to the Murnaghan equation of state (EOS) [28]. The calculated values for equilibrium lattice parameters and bulk modulus, together with other calculations [13,19] and the experimental results [15,19] are listed in Table 1. It is clear that the calculated lattice constants and bulk modulus are in good agreement with the experimental data within 3%, supporting the choices of our pseudopotentials and the GGA for the studied systems.

Figure 1 shows the calculated phonon dispersion curves of $\alpha-Li_3N$ and the projected phonon density of states (PPDOS) at different volumes. The experimental neutron inelastic scattering data (solid squares and triangles) are also shown for comparison. Besides, we explicitly present the calculated phonon frequencies of $\alpha-Li_3N$ at several special q points (e.g., Γ, K, M, and A) at zero-pressure to compare with the experimental data [29] in Table 2. It is found that the agreement between our results and the experimental data is excellent, except for the slight deviations in one optical phonon mode. With the addition of the nonanalytic term to the dynamical matrix, the longitudinal optic (LO) branch and the transverse optic (TO) branch split from each other at the Γ point, and this is also shown. It should be noted that the LO-TO splitting depends upon the direction in which one approaches the Γ point [31] and the amplitude of the splitting can be characterized by the Born effective charges tensor and the dielectric tensor, which show anisotropic characters in the case of $\alpha-Li_3N$. This leads to different behaviors of LO-TO splitting at the directions of $\Gamma - M$ and $\Gamma - A$.

Table 1. Calculated equilibrium lattice parameters a and c (Å), bulk modulus B_0 (GPa), and the pressure derivative of bulk modulus B_0' for different high pressure phases of Li_3N. Other calculations from references [13] and [19] and experimental results from references [15] and [19] are also shown for comparison.

		a(Å)	c(Å)	B_0(GPa)	B_0'
$\alpha-Li_3N$					
	This work	3.534	3.772	58.944	3.815
	Expt.15	3.648	3.875		
	reference 13	3.508	3.745	61.02	3.70
$\beta-Li_3N$					
	This work	3.445	6.148	74.503	3.412
	Expt.15	3.552	6.311		
	reference 13	3.418	6.100	78.166	3.77
$\gamma-Li_3N$					
	This work	4.870		77.096	3.541
	Expt.19	4.976		78	4.2
	reference 19	4.995		73.1	3.85

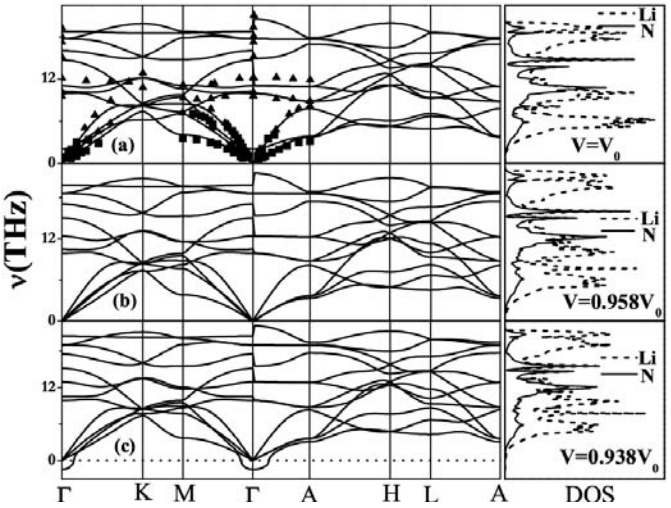

Fig. 1. The calculated phonon frequencies (left panel) and projected phonon density of states (right panel) of $\alpha-Li_3N$ at different volumes. The experimental phonon dispersion data (symbols) from reference [29] are also shown for comparison. Solid and dashed lines in the right panel are the vibrational contributions from N and Li atoms, respectively.

It is noteworthy that the calculated phonon frequency of ∼2.08 THz for the optical (B_{2g}) mode at the zone center (Γ point) is in a good agreement with the anisotropic shell-model result of ∼3.8 THz by Kress et al. [29], however, significantly lower than that of 12.11 THz calculated also by the shell model method but without including the long-range Coulomb interactions between N and Li ions by Chandrasekhar et al. [30]. This large discrepancy reflects the importance of the inclusion of the long-range Coulomb interaction in the phonon calculations. It is interesting to

Table 2. Calculated phonon frequencies (in THz unit) at the Γ, K, M, and A points of the Brillouin zone of $\alpha-Li_3N$ at zero pressure to compare with the experimental data (in curly brackets) from reference [29]. Since there are nine optical modes, it is not desirable to explicitly present the assignment of the particular modes.

Phonon modes	$\omega(\Gamma)$		$\omega(K)$		$\omega(M)$		$\omega(A)$	
Acoustic								
TA1	...		6.15		4.06	{3.57}	3.72	{3.16}
TA2	...		7.39		7.12	{7.19}	3.72	
LA	...		8.14		7.33		3.84	
Optical								
	2.08		8.14		8.47		7.79	{8.15}
	9.96	{9.52}	8.50		9.43	{9.29}	8.82	{8.87}
	10.23	{10.11}	8.50		9.78		8.82	{8.87}
	11.05	{12.13}	12.12	{12.84}	10.62		10.94	{11.85}
	14.70	{15.12}	12.12	{12.84}	11.11	{11.14}	10.94	{11.85}
	16.03		15.20		14.78		16.96	
	17.74	{18.02}	15.20		17.89		17.70	
	17.74	{18.02}	18.56		18.57		17.70	
	18.78	{19.28}	19.87		18.78		17.91	

note that the PPDOS results suggest a strong coupling feature between Li and N atomic vibrations as expected by their similar atomic masses.

With decreasing volume, the B_{2g} mode at the Γ point decreases in frequency. At a volume of 0.938 V_0 (V_0, experimental equilibrium volume), the B_{2g} mode softens to be imaginary, plotted as negative, signaling a structural instability in $\alpha-Li_3N$. The variation of the frequency of the B_{2g} mode with volume is depicted in Figure 2a. The squared phonon frequencies for the B_{2g} branch at the Γ point with pressure P are also plotted in the inset of Figure 2a. A near perfect linear relation between ν^2 and P is obtained. Such a behavior is consistent with the Landau theory of pressure-induced soft mode phase transitions [32,33]. The transition pressure corresponding to the zero phonon frequency is estimated to be 1.8 GPa from Figure 2a.

Through the analysis of the eigenvector for the softening B_{2g} mode, it is found that only the Li^+ ions of the Li_2N layers vibrate parallel to the [0001] direction as shown in the inset of Figure 2b. The stable high pressure phase can be explored by searching for the global energy minimum in the subspace spanned by the eigenvectors of the unstable mode and the additional degrees of freedom (e.g., the strain tensor) induced by the symmetry lowering due to the unstable mode. Based on the eigenvector of the softened B_{2g} mode, we distorted the original hexagonal $\alpha-Li_3N$ structure to find the appropriate atomic displacements corresponding to the lowest energy. The total energy curve in Figure 2b shows that when the external pressure is beyond around 2.5 GPa, a energy well is formed from a finite shuffle of $(11\bar{2}0)$ planes along the [0001] direction. This distortion transforms the original structure into another hexagonal phase with a lower symmetry of $P-3m1$. We name this new structure as $\alpha'-Li_3N$ depicted in the inset of Figure 5b. It is clear that the formation of $\alpha'-Li_3N$ is from the out-of-plane distortion of Li ions within the Li_2N layer. The unit cell dimension is found to be $a = 3.5315$ Å and $c = 3.7716$ Å, where Li ions occupy $1b$ (0,0,1/2) and $2d$ (1/3,2/3,z) positions, respectively, while N locates at 1a position of (0,0,0).

The precise and forceful proof on the stability of different phases of lithium nitride can be deduced from the pressure dependence of the enthalpy. In the main panel of Figure 3, the enthalpy curves for $\beta-Li_3N$ and $\gamma-Li_3N$ phases with respect to the $\alpha-Li_3N$ phase are depicted, while the $\alpha'-Li_3N$ phase has been presented in the inset of Figure 3 to make it more distinguishable. It is obvious that the $\alpha-Li_3N$ structure is the most stable ground-state structure. Above 2.8 GPa $\alpha'-Li_3N$ phase becomes energetically more favorable as indicated in the inset of Figure 3. This value is in acceptable agreement with the phase transition pressure of 1.8 GPa predicted by the phonon calculations. This new phase can stabilize up to 3.6 GPa before it transforms to $\beta-Li_3N$. At 42 GPa, the $\gamma-Li_3N$ phase is found to be stable. It is worth noting that the theoretical pressures of 3.6 and 42 GPa for the formations of $\beta-Li_3N$ and $\gamma-Li_3N$ at zero temperature, respectively, are in satisfactory agreement with the experimental measurements of 0.6 [15] and 36–45 GPa at room temperature [19]. The neglect of temperature effects in theory might be mainly responsible for this discrepancy. Note that the $\alpha'-Li_3N$

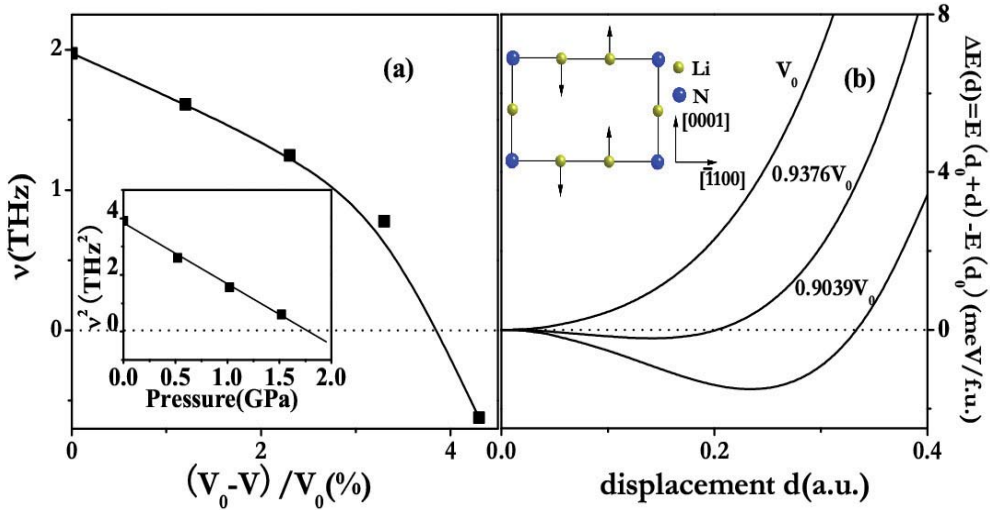

Fig. 2. (Color online) (a) Main figure: Calculated optical B_{2g} phonon frequencies at the Γ point of BZ in $\alpha-Li_3N$ as a function of volume. Solid line through the calculated data points represents the fitted curve using a B-spline. Inset: the calculated squared phonon frequency ν^2 as a function of pressure P. Solid line through the data points is a linear fit. (b) Total energy of lithium nitrides as a function of the atomic displacement of the unstable B_{2g} phonon mode in $\alpha-Li_3N$ structure. Inset shows the eigenvector of the unstable B_{2g} mode. The atomic displacements are confined in the $(11\bar{2}0)$ plane. Only the Li^+ ions in the Li_2N layers move along the [0001] direction. The arrows show the directions of atomic displacements. V_0 is the experimental equilibrium volume.

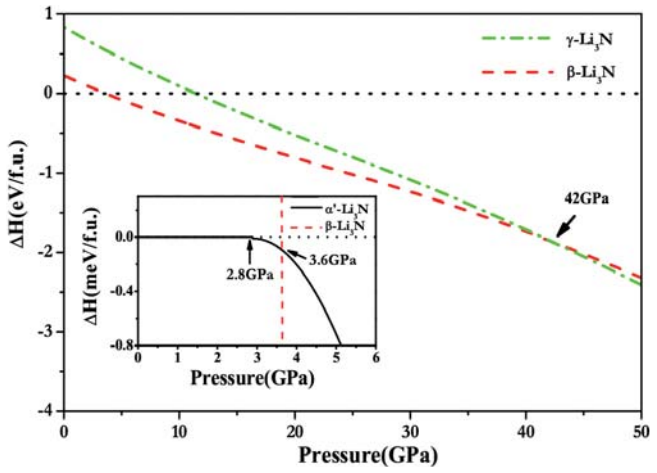

Fig. 3. (Color online) Static stability curves for the $\alpha-, \alpha'-, \beta-$ and $\gamma-Li_3N$ structures. Main figure: The enthalpy curves of $\beta-$ and $\gamma-Li_3N$ phases with respect to $\alpha-Li_3N$ structure as a function of pressure. Inset shows the enthalpy curves of $\alpha'-$ and $\beta-Li_3N$ structures with respect to $\alpha-Li_3N$ phase as a function of pressure.

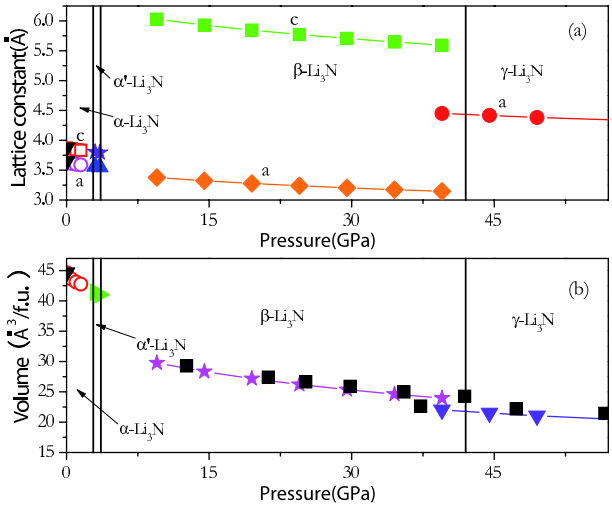

Fig. 4. (Color online) Pressure dependence of the lattice parameters (a) and the cell volumes (b) for the $\alpha-, \alpha'-, \beta-$ and $\gamma-Li_3N$ structures. Experimental lattice constants and volume (solid black triangles) of $\alpha-Li_3N$ from reference [15] at zero pressure and experimental EOS data (solid black squares) from reference [19] for $\beta-$ and $\gamma-Li_3N$ are also shown.

structure can only stabilize in a narrow pressure region of 2.8–3.6 GPa at zero temperature.

The variations of lattice parameters and the EOS with pressure for the four polymorphs are presented to compare with the experimental data (solid black squares and triangles) [15,19] in Figure 4. It is found that the theoretical volumes and EOS in different Li_3N phases are in excellent agreement with the available experimental data, supporting the validity of the theoretical model. Moreover, the lattice parameters and volume show continuous changes at the transition of $\alpha \rightarrow \alpha'$ phases characterized by the second-order nature. However, the first order phase transitions of $\alpha' \rightarrow \beta$ and $\beta \rightarrow \gamma$ are clear by evidence of obvious volume drops at the transition. It should be pointed out that there is no experimental report on the existence of $\alpha'-Li_3N$ phase. This may be resulted from that the second-order $\alpha \rightarrow \alpha'$ phase transition causes only subtle structural changes, which is difficult to be detected in the experiment. To explain this difficulty, we also simulated

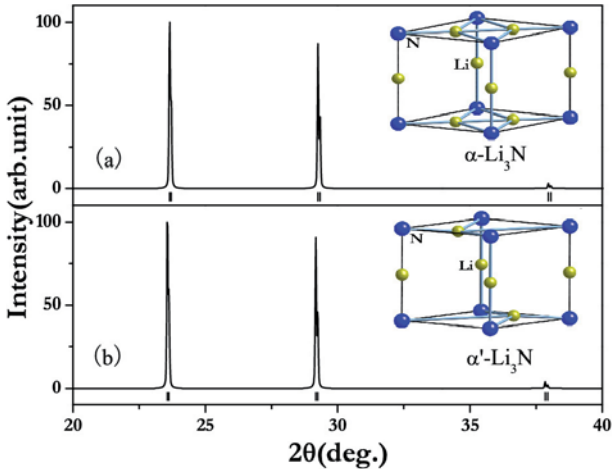

Fig. 5. (Color online) Simulated XRD patterns of (a) $\alpha-$ and (b) $\alpha'-Li_3N$ structures at 5 GPa (λ = 1.5406 Å). Inset: the crystal structures are shown with the large and small atoms representing the N and Li ions, respectively.

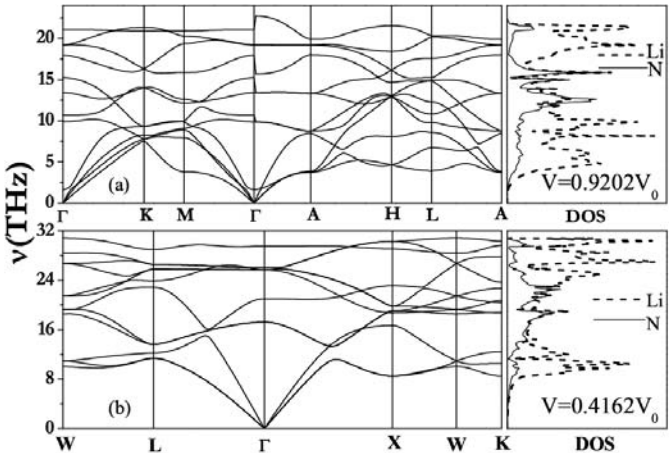

Fig. 6. (a) The calculated phonon dispersion curve (left panel) and projected phonon density of states (right panel) for $\alpha'-Li_3N$ at 4 GPa. (b) The calculated phonon dispersion curve (left panel) and projected phonon density of states (right panel) for $\gamma-Li_3N$ at 80 GPa.

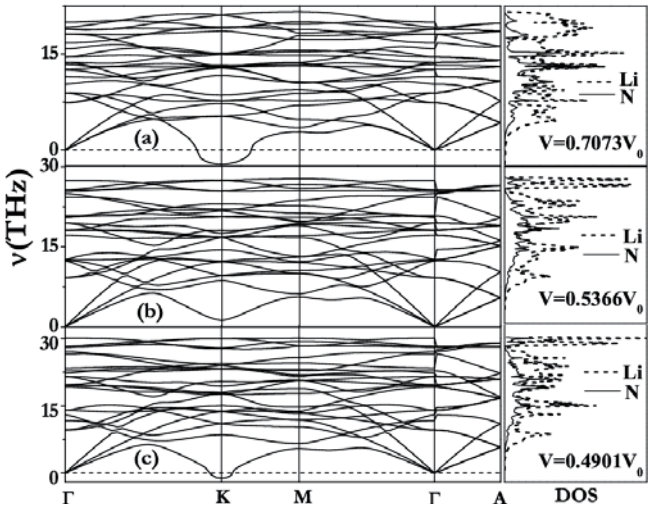

Fig. 7. The calculated phonon frequencies (left panel) and projected phonon density of states (right panel) for $\beta-Li_3N$ at different volumes.

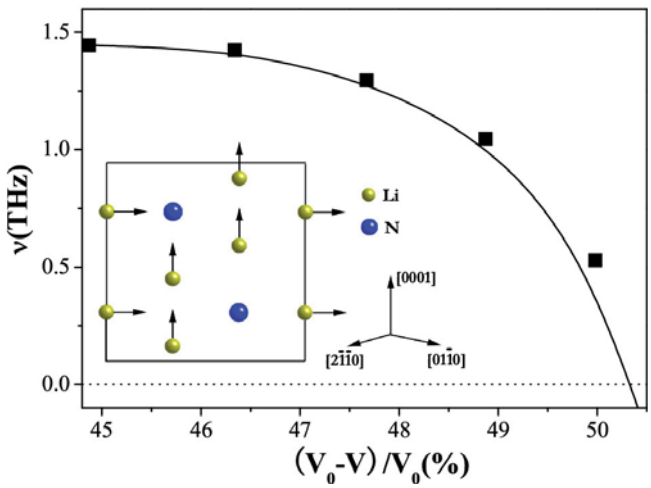

Fig. 8. (Color online) Main figure: Calculated TA (K) phonon frequencies in $\beta-Li_3N$ as a function of volume. Solid line through the calculated data points represents the fitted curve using a $B-$spline. Inset: The eigenvector for the TA soft phonon mode at K (–1/3,2/3,0) point for $\beta-Li_3N$. The displacements are all in the plane whose angle with respect to the (01$\bar{1}$0) plane is 45°. The arrows show the directions of atomic displacements.

the X-ray diffraction patterns (XRD) for the two phases in the Figure 5. It is obvious that the two XRD patterns are almost identical, except for the slight shift. In real experimental measures, the shift might be too small to be clearly observed. The lattice dynamical stability requires that the energies of phonons must be positive for all wave vectors in the BZ [32]. To further check the mechanical stability of the newly proposed $\alpha'-Li_3N$ phase, we calculate its phonon dispersion curves and PPDOS, as plotted in Figure 6a. It is found that no imaginary phonon frequency exists in the whole BZ.

Our ab initio phonon dispersion curves and PPDOS for the $\beta-Li_3N$ structure at different volumes are shown in Figure 7. At a volume of 0.71 V_0(∼5 GPa), it is obviously that the TA phonon mode at the K point is unstable (Fig. 7a). This fact is understandable since the $\beta-Li_3N$ structure is not stable in this pressure region. Interestingly, with decreasing volume to 0.54 V_0 (∼40 GPa), the TA phonon branch becomes stable. However, when the pressure increases further, the whole TA phonon branch decreases in frequency. At a volume of 0.49 V_0 (∼60 GPa), the TA phonon frequency at the K (–1/3,2/3,0) point become imaginary, signifying the structural instability in the $\beta-Li_3N$ phase. The schematic representation of eigenvectors for the soft TA phonon mode at the K point is shown in the inset of Figure 8. All the ions at the (11$\bar{2}$0) plane

are projected to the particular plane depicted in Figure 8, which forms an angle of 45° with the $(01\bar{1}0)$ plane. In this plane, the N ions at the 2c position (1/3, 2/3, 1/4) are fixed, but the Li ions at the 2b (0, 0, 1/4) and $4f$ (1/3, 2/3, z) positions vibrate along and perpendicular to the [0001] direction, respectively. With an effort to find the phase transition path of $\beta \rightarrow \gamma$, we also intended to explore the local energy minimum by displacing the atoms along the eigenvectors of the softening TA (K) phonon mode. In contrast to that in the distortion of the softening B_{2g} mode of $\alpha-Li_3N$ (Fig. 2b), we could not find the appropriate energy well. As a consequence, we failed to reveal the $\gamma-Li_3N$ structure based only on the information of the phonon softening in $\beta-Li_3N$. This fact indicates that the phase transition of $\beta \rightarrow \gamma$ is not induced independently by the phonon instability. In fact, this behavior is not surprising if one considers the first order phase transition nature of $\beta \rightarrow \gamma$. From the Landau theory, an independent soft-phonon driven phase transition renders a second order nature. While soft phonon could also drive a first order phase transition, but the strength of coupling to strain and other phonon modes becomes significant [34]. A full description of these couplings is, thus, necessary to fully understand the $\beta \rightarrow \gamma$ phase transition. Unfortunately, this kind of calculation still remains a major challenge and beyond the scope of this work. Figure 8 shows the variation of the frequency of the TA (K) branch with volume. The estimated transition pressure for phonon softening to zero frequency is 57 GPa, which is somewhat larger than the experimental transition pressure of 36–45 GPa. This fact is understandable since the transition pressure for phonon softening to zero is an upper limit.

Figure 6b presents the calculated phonon dispersions and the PPDOS for the $\gamma-Li_3N$ structure at a volume of 0.4162 V_0(∼80 GPa). No imaginary phonon frequency is observed in the whole BZ to support the dynamical stability of this phase. Notably, all the phonon modes harden with increasing pressure up to 120 GPa.

The electronic total and partial DOS for the $\alpha-$, $\alpha'-$, $\beta-$ and $\gamma-Li_3N$ structures at 0, 3, 40, and 50 GPa, respectively, are presented in Figure 9. It is found that all the phases are insulating. It is a common feature for all the compounds that the N atom has the dominant contributions to the valence band, signifying an ionic bonding nature. Moreover, the DOS changes at the $\alpha \rightarrow \alpha'$ and $\alpha' \rightarrow \beta$ transitions are relatively small, but upon entering $\gamma-Li_3N$ it is dramatic and reflects a direct confirmation of the quadrupling of the band gap at the phase transition. To our knowledge, in ionic materials the band gap is a good measure of the degree of ionicity, while the ionic materials usually appear metallic with decreasing volume. Interestingly, Li_3N is abnormal; it is found that pressure is not moving the system toward a metallic system instead the typical behavior is to broaden the band gap. Previously, it was reported [35] that the positive pressure derivative of the energy gap in diamond is understandable in terms of the absence of d occupations in the valence bands. An increase in the gap from Γ to X with pressure in the zinc-blende BN [36] might also have the same origin.

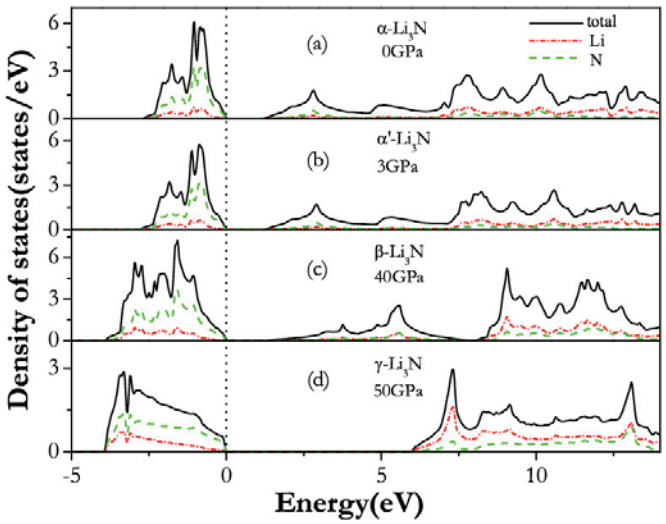

Fig. 9. (Color online) Calculated electronic total and partial densities of states for (a) $\alpha-$, (b) $\alpha'-$, (c) $\beta-$ and (d) $\gamma-Li_3N$ at 0, 3, 40 and 50 GPa, respectively. Vertical dotted lines indicate the Fermi energy.

Here, in view of the apparent d states shortage in Li_3N, one might expect a similar understanding of the band gap broadening.

4 Conclusion

In summary, we have investigated the structural phase transition and electronic properties of Li_3N under pressure through the first-principles calculations. Within the GGA calculations, we predicted that the $\alpha-Li_3N$ will transform to the hexagonal $\alpha'-$phase at 2.8 GPa at zero temperature. We invite future experimental XRD and Raman measurements to verify the existence of this phase. With increasing pressure, the phase transitions of $\alpha' \rightarrow \beta$ and $\beta \rightarrow \gamma$ are characterized by the first order nature with the sharp reduction of volumes at the transformations, in agreement with experimental results. We show that the second order phase transition of $\alpha \rightarrow \alpha'$ is induced by phonon instabilities, while the transition of $\beta \rightarrow \gamma$ may be driven through coupling of unstable modes to strain. Based on the calculated total and partial DOS, we conclude that four high pressure forms of Li_3N are all ionic compounds. The typical pressure effect is found to broaden the energy gap.

We thank the financial support of the China 973 Program under grant No. 2005CB724400, the NSAF of China under Grant No.10676011, the National Doctoral Foundation of China Education Ministry under Grant No. 20050183062, the SRF for ROCS, SEM, the Program for 2005 New Century Excellent Talents in University, and the 2006 Project for Scientific and Technical Development of Jilin Province. Most of calculations in this work have been done using the Quantum-ESPRESSO package [21].

References

1. A. Rabenau, in *Festkörperprobleme* (Advances in Solid State Physics) edited by J. Treusch (Vieweg, Braunschweig, 1978), vol. 18, p. 77
2. B.A. Boukamp, R.A. Huggins, Mater. Res. Bull. **13**, 23 (1978)
3. R.A. Huggins, A. Rabenau, Mater. Res. Bull. B **13**, 1315 (1978)
4. M.L. Wolf, J. Phys. C **17**, L285 (1984)
5. J. Sarnthein, K. Schwarz, P.E. Blöchl, Phys. Rev. B **53**, 9084 (1996)
6. E. Bechtold-Schweickert, M. Mali, J. Roos, D. Brinkmann, Phys. Rev. B **30**, 2891(1984)
7. A. Rabenau, H. Schulz, J. Less Common Metals **50**, 155 (1976); A. Rabenau, Solid State Ionics **6**, 277 (1982)
8. P. Chen, Z. Xiong, J. Luo, J. Lin, K. Lee Tan, Nature (London) **420**, 302 (2002)
9. T. Ichikawa, S. Isobe, N. Hanada, H. Fujii, J. Alloys Compd. **365**, 271 (2004)
10. Yun Hang Hu, Eli Ruckenstein, Ind. Eng. Chem. Res. **44**, 1510 (2005)
11. Y. Nakamori, G. Kitahara, K. Miwa, S. Towata, S. Orimo, Appl. Phys. A: Mater. Sci. Process. **80**, 1 (2005)
12. Y. Xie, Y. Qian, W. Wang, S. Zhang, Y. Zhang, Science **272**, 1926 (1996)
13. A.C. Ho, M.K. Granger, A.L. Ruoff, P.E. Van Camp, V.E. Van Doren, Phys. Rev. B **59**, 6083 (1999)
14. E. Zintl, G. Bauer, Z. Elektrochem. **41**, 102 (1935)
15. H.J. Beister, Sabine Haag et al., Angew. Chem, Int. Ed. Engl. **27**, 1101 (1988)
16. G. Kerker, Phys. Rev. B **23**, 6312 (1981)
17. R. Dovesi, C. Pisani, F. Ricca, C. Roetti, V.R. Saunders, Phys. Rev. B **30**, 972 (1984)
18. J.C. Schön, M.A.C. Wevers, M. Jansen, J. Mater. Chem. **11**, 69 (2001)
19. A. Lazicki, B. Maddox, W.J. Evans, C.S. Yoo, A.K. McMahan, W.E. Pickett, R.T. Scalettar, M.Y. Hu, P. Chow. Phys. Rev. Lett. **95**, 165503 (2005)
20. P. Hohenberg, W. Kohn, Phys. Rev. **136**, 864 (1964); W. Kohn, L.J. Sham, Phys. Rev. A **136**, 1133 (1965)
21. S. Baroni, A. Dal Corso, S. de Gironcoli, P. Giannozzi, C. Cavazzoni, G. Ballabio, S. Scandolo, G. Chiarotti, P. Focher, A. Pasquarello, K. Laasonen, A. Trave, R. Car, N. Marzari, A. Kokalj, http://www.pwscf.org
22. J.P. Perdew, K. Burke, Int. J. Quantum Chem. **57**, 309 (1996); J.P. Perdew, K. Burke, M. Ernzerhof, Phys. Rev. Lett. **77**, 3865 (1996)
23. N. Troullier, J.L. Martins, Phys. Rev. B **43**, 1993 (1991)
24. H.J. Monkhorst, J.D. Pack, Phys. Rev. B **13**, 5188 (1976)
25. S. Baroni, P. Giannozzi, A. Testa, Phys. Rev. Lett. **58**, 1861 (1987); P. Giannozzi, S. de Gironcoli, P. Pavone, S. Baroni, Phys. Rev. B **43**, 7231 (1991)
26. S. de Gironcoli, Phys. Rev. B **51**, 6773 (1995)
27. V. Ozoliņš, Ph.D. thesis, Royal Institute of Technology, Sweden, 1996
28. F.D. Murnaghan, Proc. Natl. Acad. Sci. USA. **30**, 244 (1944)
29. W. Kress, H. Grimm, W. Press, J. Lefebvre, Phys. Rev. B **22**, 4620 (1980)
30. H.R. Chandrasekhar, G. Bhattacharya, R. Migoni, H. Bilz, Phys. Rev. B **17**, 884 (1978)
31. N.W. Ashcroft, N.D Mermin, *Solid State Physics* (HRM International Editions, Phyiladelphia 1976) p. 548
32. G.A. Samara, P.S. Peercy, in Solid State Physics, edited by H. Ehrenreich, F. Seitz, D. Turnbull (Academic, New York, 1981), vol. 36
33. W. Von der Osten, B. Dorner, Solid State Commun. **16**, 431 (1975)
34. X. Huang, K.M. Rabe, G.J. Ackland, Phys. Rev. B **67**, 024101 (2003)
35. S. Fahy, K.J. Chang, S.G. Louie, M.L. Cohen, Phys. Rev. B **35**, 5856 (1987)
36. R.M. Wentzcovitch, K.J. Chang, M.L. Cohen, Phys. Rev. B **34**, 1071 (1986)